高压物理学报
CHINESE JOURNAL OF HIGH PRESSURE PHYSICS

第 32 卷 第 3 期
2018 年 6 月

高 压 物 理 学 报
CHINESE JOURNAL OF HIGH PRESSURE PHYSICS

Vol. 32, No. 3
June, 2018

DOI: 10.11858/gywlxb.20170624

Numerical Investigations of Perturbation Growth in Aluminum Flyer Driven by Explosion*

WANG Tao[1,2], BAI Jingsong[1], CAO Renyi[1], WANG Bing[1], ZHONG Min[1], LI Ping[1], TAO Gang[2]

(1. *Institute of Fluid Physics, CAEP, Mianyang* 621999, *China*;
2. *School of Energy and Power Engineering, Nanjing University of Science and Technology, Nanjing* 210094, *China*)

Abstract: In this paper we developed an experimental technique and numerical simulation method that we then adopted to investigate the Rayleigh-Taylor instability in metallic materials driven by explosion. We studied experimentally and numerically the growth of the Rayleigh-Taylor instability in an explosion-driven aluminum flyer and showed that the perturbation amplitude growth follows an exponential law over time. The numerical results agree with the experiment qualitatively, but not quantitatively. This is because the aluminum strengthens under high pressure and at high strain rate, and the Steinberg-Guinan constitutive model used in the simulations underestimates the strength of the aluminum as being not great enough to suppress the perturbation growth. By investigating numerically the effects of the initial shear modulus and the initial yield strength on the development of the Rayleigh-Taylor instability of the metallic material, we also found that the initial shear modulus in a specified range does not affect the dynamic yield strength and the increase in the initial yield strength can improve the dynamic yield strength significantly to stabilize the perturbation growth. In other words, the material strength dominates the interface perturbation growth.

Keywords: explosion-driven; Rayleigh-Taylor instability; perturbation growth; material strength; stabilize

CLC number: O33; O344.3 **Document code**: A

The corrugated interface between different fluids grow when accelerated from a low-density fluid to a high-density fluid, which is called Rayleigh-Taylor (RT) instability[1-2]. This phenomenon may also occur in metals, but usually under a high pressure and at a high strain-rate, but differs most distinctly from the RT instability in fluids in its strength effect of the metal, which can stabilize the perturbation growth[3-4] and make the metallic RT instability more complex and difficult. Here, it is also affected by the loading state and the properties of the metallic materials. The metallic RT instability at high pressure and strain-rate can be observed in inertial confinement fusion[5], supernova explosion[6], asteroid collision[7], the motion of earth's inner core and plate tectonics[8], and so on. Therefore, the metallic RT instability is currently a major concern for researchers and receives a great deal of academic attention.

In theoretical studies about the metallic interface instability, dispersion relations of the perturbation growth are derived mainly based on the energy[9-11] or force equilibrium[12-13]. However, the previous

* **Received date**: 2017-08-01; **Revised date**: 2017-08-30

Foundation Item: Science Challenge Project (TZ2016001); National Natural Science Foundation of China (11372294, 11532012, 11672277)

Biography: WANG Tao (1979—), male, master, major in computational mechanics. E-mail: wtao_mg@163.com

linear analysis cannot predict the perturbation growth accurately just by applying the perfect plastic constitutive relation and constant pressure loading state. Based on the energy balance, a perturbation growth equation using Steinberg-Guinan (SG) and the Johnson-Cook constitutive models, as well as a variable pressure loading process consistent with experiments, has been derived that precisely predicts the growth of metallic RT instabilities driven by detonation and laser plasma. However, the linear analysis still has its limitations and does not take full account of the loading procedure.

Experimental studies of the metallic RT instability started in the 1970s. The pioneering experimental research[14] was the perturbation growth of a flat aluminum plate accelerated by the expansion of detonation products, which was observed using a high-energy X-ray facility. What was achieved then inspired researchers, and the similar equipment was utilized in later research[15-17]. In the USA and Russia particularly, numerous numerical simulations and experimental investigations for the metallic RT instability have been carried out, but have mainly concentrated on the perturbation growth and such influencing factors as the initial amplitude, the wavelength and material properties. Igonin and Ignatova *et al.*[18-19] experimentally and numerically studied the dynamic behaviors of copper (Cu) and tantalum (Ta) subjected to both shock and shockless loading by employing a perturbation growth method. They observed that the formation of the bi-periodic twin structures resulted in an initial loss of the shear strength of Cu, but failed to observe localization in Ta. Olson *et al.*[16] experimentally studied the effects of the grain size and material processing on the RT perturbation growth of Cu. They found that both the single-crystal orientation and the strain hardening due to the material processing can affect the perturbation growth, but the polycrystalline grain size cannot. For the plane detonation, the loading pressure is generally about 30 GPa. To enhance the loading pressure, Henry de Frahan *et al.*[17] studied the beryllium RT instability using an iron flyer plate to impact the second high explosive (HE) to raise the pressure to 50 GPa in their experiments, and combined numerical simulations to calibrate the feasibility of different constitutive models. When the sample is driven by electromagnetism[20-21] or laser[4,22], the loading pressure can be further increased. Very extreme conditions of pressures over 1000 GPa and strain rates of 10^8 s^{-1} have been achieved at the National Ignition Facility, USA, where the RT instability experiment in vanadium was carried out, and constitutive models in solid phase were tested by comparing simulations with experiments measuring the perturbation growth[23] under the extreme conditions mentioned.

In the metallic interface instability, the perturbation growth is related to and arrested by the material strength. Moreover, some investigations have demonstrated that the material strength increases under these extreme conditions. Results from the metallic RT experiments and computations by Barnes *et al.*[14] show that the yield strength of 1100-0 aluminum is over 10 times larger than the standard parameter, and the yield strength of 304 stainless steel also increases by more than three times. Using the SG constitutive strength model, calculations of plasma-driven quasi-isentropic RT experiments of Al-6061-T6 using the Omega laser at a peak drive pressure of 20 GPa indicate that its yield strength is a factor of about 3.6 times over the ambient value[22]. In Park *et al.*'s[4] plasma-driven quasi-isentropic polycrystalline vanadium RT experiments using the Omega laser with a peak drive pressure of 100 GPa, the measured RT growth was substantially lower than predictions using the existing constitutive models (SG and Preston-Tonks-Wallace) that work well at low pressures and long timescales. Using the SG model, the simulations agree with the RT experimental data when the initial strength is raised by a factor of 2.3. Therefore, the SG and Preston-Tonks-Wallace models underestimate the strength of vanadium under very high pressures and strain rates. Belof *et al.*[24] first meas-

ured the dynamic strength of iron undergoing solid-solid phase transition by using RT instability. In conjunction with detailed hydrodynamic simulations, the analysis results revealed significant strength enhancement of the dynamically generated ε-Fe and reverted α'-Fe, comparable in magnitude to the strength of austenitic stainless steels. Therefore, the metallic RT instability was suggested and used as a tool for evaluating the material strength of solids at high pressures and high strain rates[3,25], and then for modifying or developing new constitutive models for these conditions[26-27].

In view of the dominant role of the material strength in metallic interface instabilities, and the limitations of existing constitutive models at high pressures and high strain rates, we aimed to investigate the material strength and its effects on metallic interface instabilities. In this paper, we also conducted an RT instability experiment in explosion-driven aluminum, and measured the perturbation growth using X-ray radiography. In combination with elastic-plastic hydrodynamic simulations, we investigated the dynamic behavior of metallic RT instabilities and the role of the material strength in these.

1　Experimental Setup

Following that of Barnes *et al.*,[14] our experiment used the setup as shown in Fig. 1(a), where we have a sketch of the experimental setup consisting of a detonator, a booster, plane wave lens, JO-9159 HE (100 mm in diameter and 50 mm in thickness), an aluminum sample, and a vacuum. Fig. 1(b) shows the experimental sample of aluminum with a diameter of 65 mm and a thickness of 1.5 mm in the central region. An initial sinusoidal perturbation was machined on the side of the aluminum sample facing the HE. The perturbation amplitude and wavelength were 0.25 mm and 6 mm, respectively. The HE products crossed the void of 3.5 mm between the sample and HE and accumulated on the perturbation interface of the sample, providing a smooth rise to peak pressure and a quasi-isentropic drive. Moreover, the void between the sample and HE can ensure that the temperature of the sample at high pressures remain below the melting point[22].

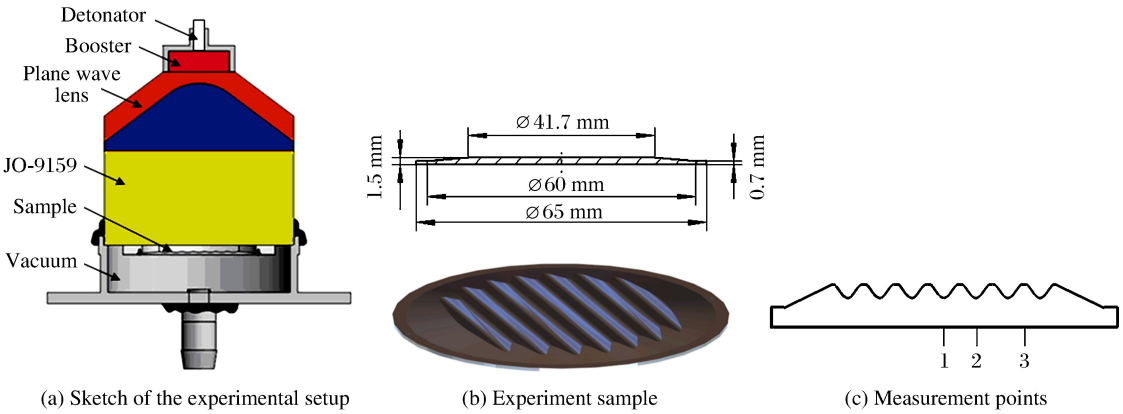

Fig. 1　Sketch of the experimental setup and sample

In the experiment, X-ray radiography was used to record the evolution of the perturbation interface from the JO-9159 explosive detonation at zero time. A Doppler pin system was used to measure the history of the free surface velocity, which can be integrated to obtain the corresponding free surface displacement. Fig. 1(c) shows the distribution of measurement points of the free surface velocity, where both points 1 and 2 correspond to the wave trough positions with one wavelength interval, and point 3 corresponds to the wave crest position with 1.5 wavelength intervals from point 2.

2 Numerical Methods

Based on our indoor hydrodynamic code of compressible multi-viscous flow and turbulence (MVFT)[28-30], we developed a detonation and shock dynamics code with high fidelity by considering the explosive detonation and the elastic-plastic behavior of the material. This code can be used to study the physical problem of multi-materials, large deformation, and strong shock. The governing equations in conserved form are as follows

$$\begin{cases} \dfrac{\partial}{\partial t}\displaystyle\int_V \rho \mathrm{d}V = -\oint_S \rho u_i n_i \mathrm{d}S \\ \dfrac{\partial}{\partial t}\displaystyle\int_V \rho u_j \mathrm{d}V = -\oint_S P n_j \mathrm{d}S - \oint_S \rho u_i u_j n_i \mathrm{d}S + \oint_S s_{ij} n_i \mathrm{d}S \\ \dfrac{\partial}{\partial t}\displaystyle\int_V \rho E \mathrm{d}V = -\oint_S u_i P n_i \mathrm{d}S - \oint_S \rho u_i E n_i \mathrm{d}S + \oint_S s_{ij} u_j n_i \mathrm{d}S \end{cases} \tag{1}$$

where i and j represent the x, y, and z directions; V is the control volume, S the surface of control volume, n the unit vector of the external normal direction, ρ, u_k (where $k=i,j$), p, and E are the density, velocity, pressure, and total energy of per unit mass; and s_{ij} the deviation stress tensor.

The physical problem as described by Eq. (1) was decomposed into three one-dimensional problems. For each of them, the physical quantities in a cell were interpolated and reconstructed using a piecewise parabolic method (PPM). The one-dimensional problem was then resolved using a two-step Euler algorithm: First the physical quantities were solved by the Lagrange matching, and then remapped back to the stationary Euler meshes. The effect of material strength, explosive detonation, and artificial viscosity were implemented in the Lagrange step. The multi-material interface was captured by applying a volume-of-fluid (VOF) method.

2.1 Equation of State

In our numerical simulations, the equation of state (EOS) for the explosive and aluminum are the Jones-Wilkins-Lee (JWL) and Mie-Grüneisen equations of state, respectively. The Jones-Wilkins-Lee equation of state is

$$p(\rho,T) = A\left(1-\frac{\omega}{R_1 v}\right)\mathrm{e}^{-R_1 v} + B\left(1-\frac{\omega}{R_2 v}\right)\mathrm{e}^{-R_2 v} + \frac{\omega \bar{E}}{v} \tag{2}$$

where $v=\rho_0/\rho$ is specific volume; A, B, R_1, R_2, and ω are constants; and $\bar{E}$ is the internal energy per unit volume. Table 1 lists the JWL EOS parameters of the JO-9159 explosive. The Mie-Grüneisen equation of state is

$$p = \frac{\rho_0 c^2 \mu\left[1+(1-\gamma_0/2)\mu - a\mu^2/2\right]}{\left[1-(S_1-1)\mu - \dfrac{S_2\mu^2}{\mu+1} - \dfrac{S_3\mu^3}{(\mu+1)^2}\right]^2} + (\gamma_0 + a\mu)\bar{E} \tag{3}$$

where $\mu=\rho/\rho_0-1$ is the relative compression, ρ_0 the initial density, c the sound velocity at zero pressure, γ_0 the Grüneisen coefficient, and a, S_1, S_2, and S_3 are constants (in Table 2).

Table 1　Equation of state parameters of JO-9159 explosive

ρ/(g·cm^{-3})	p_{CJ}/GPa	D_{CJ}/(km·s^{-1})	A/GPa	B/GPa	R_1	R_2	ω
1.86	36	8.862	934.8	12.7	4.6	1.1	0.37

Table 2　Mie-Grüneisen equation of state parameters of aluminum

ρ/(g·cm^{-3})	c/(km·s^{-1})	γ_0	a	S_1	S_2	S_3
2.703	5.22	1.97	0.47	1.37	0	0

2.2 Constitutive Model

In our simulations, the elastic-plastic behavior of aluminum at high pressures and high strain rates was described using the SG constitutive model. The SG model introduces pressure, temperature, and strain-rate terms into the elastic-plastic constitutive equation, while the coupling effect of pressure and strain rate on flow stress was characterized by the separating variables. Additionally, as the flow stress in the SG model relies on pressure, there is a coupling relationship between the material constitutive equation and the equation of state, which indicates the feature of pressure hardening of metal under high pressure. The dynamic yield strength Y_{SG} and the shear modulus G determined by the SG model are expressed as

$$Y_{SG} = Y_0 \ [1 + \beta(\varepsilon_p + \varepsilon_i)]^n [1 + Ap\eta^{-1/3} - B(T - 300)] \tag{4}$$

$$G = G_0 [1 + Ap\eta^{-1/3} - B(T - 300)] \tag{5}$$

where Y_0 and G_0 are the initial yield strength and the shear modulus, respectively; β and n are the material strain hardening coefficient and the hardening index, respectively; A is the pressure hardening coefficient; $\eta = \rho/\rho_0$ is the material compression ratio; and B is the temperature softening coefficient (in Table 3).

Table 3　Steinberg-Guinan constitutive model parameters of aluminum

Y_0/GPa	Y_{max}/GPa	G_0/GPa	β	n	A/GPa^{-1}	B/(10^{-3}K^{-1})
0.29	0.68	27.6	125	0.1	0.0652	0.616

3 Results and Discussions

In our experiment, X-ray radiography recorded an image of the perturbed interface at 7.78 μs, as shown in Fig. 2(a), from which we obtained the amplitude of 0.77 mm simultaneously by image processing. In the simulations, the mesh size was 15.6 μm, and Tables 2 and 3 list the parameters of the Mie-Grüneisen EOS and the SG constitutive model of aluminum, respectively.

(a)　(b)　(c)

Fig. 2　Comparisons of the perturbed interface between experiment and numerical simulations ((a) Experimental image, (b) Simulated image at normal strengths Y_0 and G_0, (c) Simulated image at 10 times the normal strengths Y_0 and G_0)

Fig. 3 shows the pressure histories of the crest (solid line) and the trough (dashed line) on the loading surface, which increase continuously and smoothly in a short time and form an approximate quasi-isentropic drive. Afterwards, the expansion of the detonation products decelerates gradually, and the loading pressure on the interface rises slowly. However, the pressure at the trough ascends faster than that at the crest, and the peak pressure at the trough is also relatively larger, because the detonation products converges at the trough and diverges at the crest. The average peak

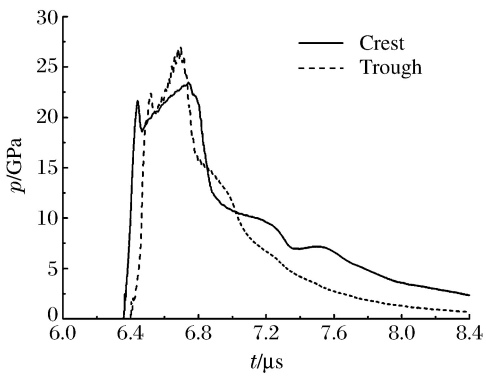

Fig. 3　Pressure histories of crest and trough at the loading surface

pressure is about 25 GPa, and the strain rate reaches 10^6 s^{-1}. The loading pressure then reduces gradually, which is attributed to the decrease of the expansion pressure of the detonation products and the unloading effect of the rarefaction wave reflecting from the free surface.

Fig. 4 shows several contours of local pressure (a), density (b), and temperature (c) at 6 different times after the arrival of the detonation products at the loading surface, from left to right and top to bottom, at 6.36, 6.5, 6.7, 6.9, 7.1 and 7.3 μs. They exhibit an evolution process of the perturbed interface and the interaction of the wave and the interface. The blue part of the temperature contour is the aluminum sample, and the sample temperature remains below 500 K and far below the melting point of 1 200 K, which indicates that the sample is in the elastic-plastic state all the time.

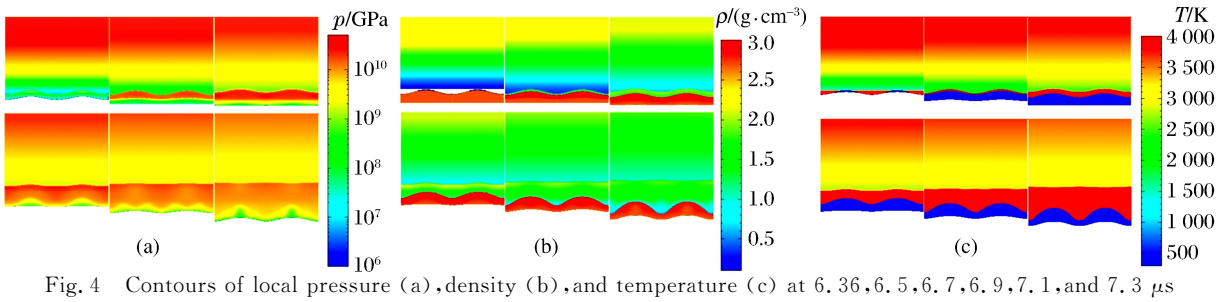

Fig. 4　Contours of local pressure (a), density (b), and temperature (c) at 6.36, 6.5, 6.7, 6.9, 7.1, and 7.3 μs from left to right and top to bottom after the arrival of detonation products at the loading surface

Fig. 2(b) shows an image of the sample at 7.78 μs when the initial yield strength Y_0 and the shear modulus G_0 are normal values. Fig. 5 shows a comparison of the perturbation amplitudes between the experiment and numerical simulations, where the square symbol corresponds to the experimental result, and the solid black line corresponds to the numerical results when Y_0 and G_0 are normal. The simulated amplitude is much larger than that in the experiment when using normal values of Y_0 and G_0. This is because the aluminum strengthens under such conditions, and the SG constitutive model underestimates its strength, which can suppress the perturbation growth.

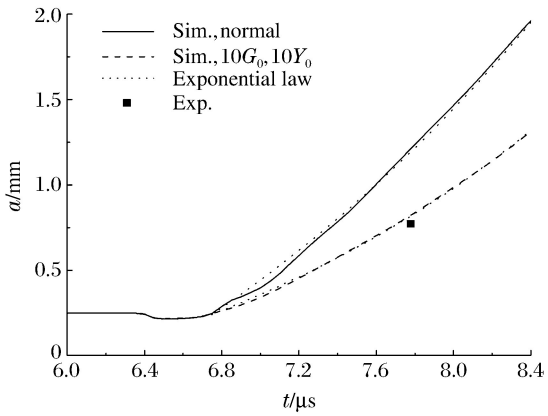

Fig. 5　Growth histories of the perturbation amplitude

Fig. 6 shows the time histories of the free surface velocity (a) and displacement (b) at 3 measurement points (dot-dot-dashed lines: experiment; solid, dashed, and dotted lines: simulations), which agree well with each other. Therefore, the calculations of detonation of the explosive and the thermodynamic state of the sample are exact.

Fig. 7 shows the calculated time histories of the strain at the crest (solid line) and trough (dashed line) of the loading surface. The deformation at the trough is much larger than that at the crest because the trough of the sample is in a stronger tensile stress state, which is the main mechanism for the deformation of the perturbation interface. Fig. 8 shows the time histories of the dynamic yield strength at the crest (solid line) and trough (dashed line) of the loading surface, calculated using the SG constitutive model, similar to the profile of the loading pressure, which demonstrate that the material strength increased as did the loading pressure under a certain condition.

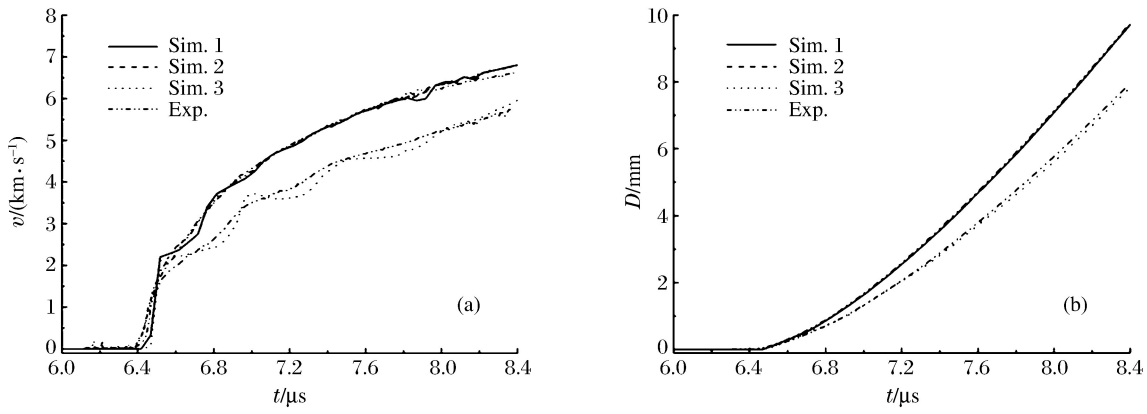

Fig. 6　Time histories of the free surface velocity (a) and displacement (b)

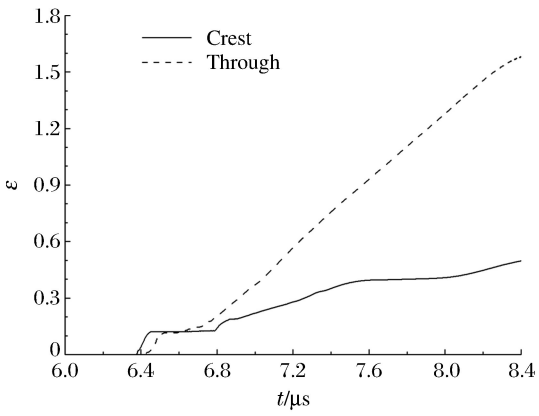

Fig. 7　Time histories of strain at the crest and trough of the loading surface

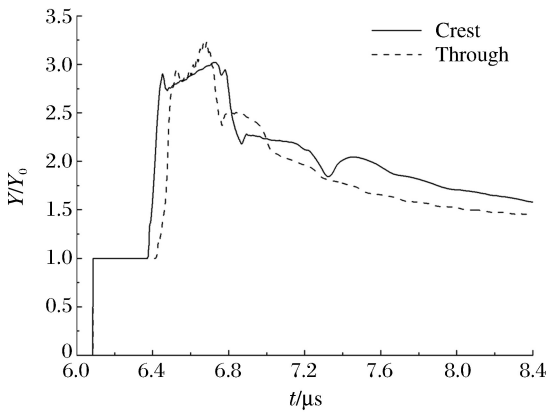

Fig. 8　Time histories of yield strength at the crest and trough of the loading surface

Moreover, when the loading pressure reaches a peak, the dynamic yield strength was up to 3 times that of the initial value. In fact, the normal SG model is generally calibrated by conventional Hopkinson and Taylor impacts experiment with a lower strain rate. Under the current loading conditions (loading pressure of 25 GPa and strain rate of 10^6 s^{-1}), the strength is not great enough to suppress the perturbation growth. However, when the initial yield strength Y_0 and the shear modulus G_0 increase to 10 times that of the normal values, good agreement between the experiment and simulation is achieved, as shown in Fig. 2(c) for the perturbation interface and in Fig. 5 for the perturbation amplitude with the dashed line. Therefore, the material strength intensively stabilizes the perturbation growth. The dotted lines in Fig. 5 are fitted lines from the simulated results, indicating that the perturbation amplitude grows exponentially over time.

We studied the effect of the initial yield strength and the initial shear modulus of the material on the evolution and growth of the perturbed interface. Figs. 9(a), 10(a), and 11(a) show the calculated growth histories of perturbation amplitude, strain histories, and dynamic yield strength histories at the trough of the loading surface, respectively, when the initial yield strength is fixed at the normal value and as the initial shear modulus increases gradually. The growth of the perturbation amplitude exhibits no change even when the initial shear modulus increases to 10 times that of the normal value, which means that the initial shear modulus has no influence on the material deformation and does not affect

the dynamic yield strength.

Figs. 9(b), 10(b), and 11(b) show the numerical results when the initial shear modulus is fixed and the initial yield strength gradually increases to 10 times that of the normal value. These indicate that, with the increase of the initial yield strength, the dynamic yield strength also increases, the material deformation is retarded, and the perturbation growth is suppressed markedly. Therefore, the initial shear modulus of the material exerts no effect on the growth of the metallic RT instability within a certain range, while the initial yield strength has an obvious effect on it.

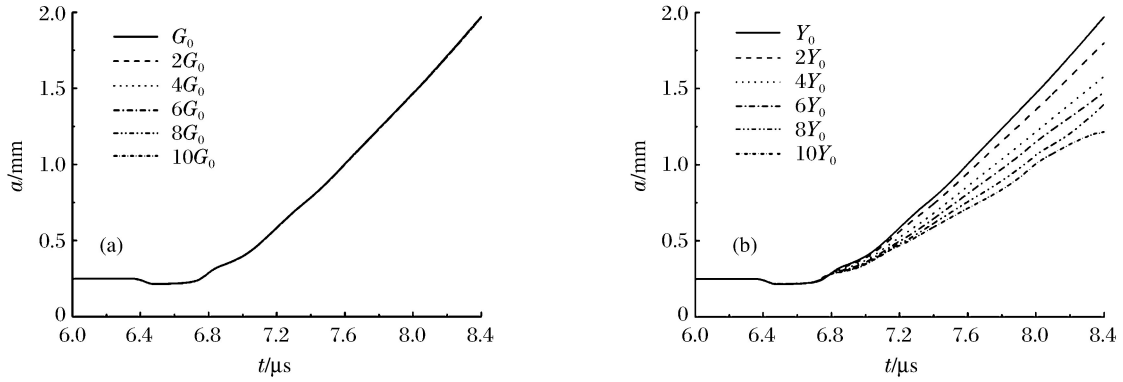

Fig. 9　Growth histories of the perturbation amplitude for different values of initial shear modulus (a) and yield strength (b)

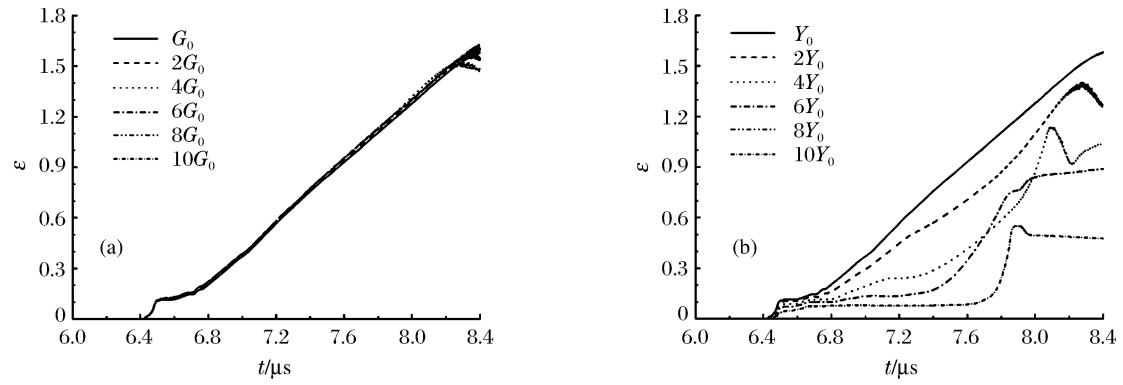

Fig. 10　Time histories of strain at the trough of the loading surface for different values of initial shear modulus (a) and yield strength (b)

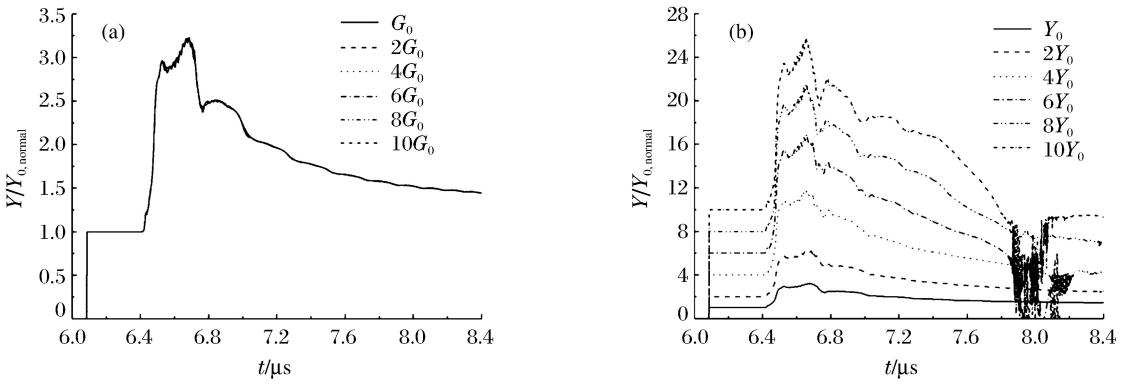

Fig. 11　Time histories of yield strength at the trough of the loading surface for different values of initial shear modulus (a) and yield strength (b)

4 Conclusions

We have established an experimental setup and developed a numerical simulation method to investigate the RT instability in metallic materials driven by explosion. We also studied the RT instability in aluminum, and drew the following conclusions:

(1) The perturbation amplitude grows following an exponential law over time.

(2) When using the normal physical property parameters of aluminum, simulated evolution of the perturbed interface agrees with experiment only qualitatively, and there is a big quantitative difference between them because the aluminum strengthens under high pressures and at high strain rates, and the SG constitutive model underestimates its strength as being not great enough to suppress the perturbation growth.

(3) When the initial yield strength and the initial shear modulus increase to 10 times their normal values, the numerical and experimental results are in good agreement both qualitatively and quantitatively. The underlying physical mechanism is the stabilization effect of material strength on the perturbation growth. Moreover, the initial shear modulus has no influence on the perturbation growth within a certain range whereas the initial yield strength does influence it strongly. Therefore, the material strength dominates the evolution of the metallic RT instability.

References:

[1] RAYLEIGH L. Investigation of the character of the equilibrium of an incompressible heavy fluid of variable density [J]. Proceedings London Mathematical Society, 1883, 14(1): 170-177.

[2] TAYLOR G I. The instability of liquid surfaces when accelerated in a direction perpendicular to their plane [J]. Proceedings of the Royal Society of London, Series A, 1950, 201(1065): 192-196.

[3] DIMONTE G, TERRONES G, CHERNE F J, et al. Use of the Richtmyer-Meshkov instability to infer yield stress at high-energy densities [J]. Physical Review Letters, 2011, 107(26): 264502.

[4] PARK H S, REMINGTON B A, BECKER R C, et al. Strong stabilization of the Rayleigh-Taylor instability by material strength at megabar pressures [J]. Physics of Plasmas, 2010, 17(5): 056314.

[5] MCCRORY R L, MONTIERTH L, MORSE R L, et al. Nonlinear evolution of ablation-driven Rayleigh-Taylor instability [J]. Physical Review Letters, 1981, 46(5): 336-339.

[6] KIFONIDIS K, PLEWA T, SCHECK L, et al. Non-spherical core collapse supernovae Ⅱ. The late-time evolution of globally anisotropic neutrino-driven explosions and their implications for SN 1987A [J]. Astron Astrophys, 2006, 453: 661-678.

[7] MAC LOW M M, ZAHNLE K. Explosion of comet shoemaker-levy 9 on entry into the jovian atmosphere [J]. The Astrophysical Journal, 1994, 434: L33-L36.

[8] MOLNAR P, HOUSEMAN G A, CONRAD C P. Rayleigh-Taylor instability and convective thinning of mechanically thickened lithosphere: effects of non-linear viscosity decreasing exponentially with depth and of horizontal shortening of the layer [J]. Geophysical Journal International, 1998, 133(3): 568-584.

[9] MILES J W. Taylor instability of a flat plate, General atomic division of general dynamics: GAMD-7335 [R]. 1966.

[10] WHITE G N. A one-degree-of-freedom model for the Tayloy instability of an ideally plastic metal plate: LA-5225-MS [R]. Los Alamos, NM: Los Alamos National Laboratory, 1973.

[11] ROBINSON A C, SWEGLE J W. Acceleration instability in elastic-plastic solids II. Analytical techniques [J]. Journal of Applied Physics, 1989, 66(7): 2859-2872.

[12] PIRIZ A R, LÓPEZ CELA J J, CORTÁZAR O D, et al. Rayleigh-Taylor instability in elastic solids [J]. Physical Review E, 2005, 72(5): 056313.

[13] PIRIZ A R,LÓPEZ CELA J J,TAHIR N A. Rayleigh-Taylor instability in elastic-plastic solids [J]. Journal of Applied Physics,2009,105(11):116101.

[14] BARNES J F,BLEWETT P J,MCQUEEN R G,et al. Taylor instability in solids [J]. Journal of Applied Physics,1974,45(2):727-732.

[15] GRAHAM L M J,CAVALLO R M,LORENZ K T,et al. Aluminum Rayleigh Taylor strength measurements and calculations [C]//10th International Workshop on Physics of Compressible Turbulent Mixing. Paris,France,2006.

[16] OLSON R T,CERRETA E K,MORRIS C,et al. The effect of microstructure on Rayleigh-Taylor instability growth in solids [J]. Journal of Physics:Conference Series,2014,500:112048.

[17] HENRY DE FRAHAN M T,BELOF J L,CAVALLO R M,et al. Experimental and numerical investigations of beryllium strength models using the Rayleigh-Taylor instability [J]. Journal of Applied Physics,2015,117(22):225901.

[18] APRELKOV O N,IGNATOVA O N,IGONIN V V,et al. Twinning and dynamic strength of copper during high-rate strain [C]//Shock Compression of Condensed Matter—AIP Conference Proceedings,2007,955(1):619-622.

[19] IGONIN V V,IGNATOVA O N,LEBEDEV A I,et al. Influence of dynamic properties on perturbation growth in tantalum [C]//Shock Compression of Condensed Matter—AIP Conference Proceedings,2010,1195(1):1085-1088.

[20] SLUTZ S A,HERRMANN M C,VESEY R A,et al. Pulsed-power-driven cylindrical liner implosions of laser preheated fuel magnetized with an axial field [J]. Physics Plasmas,2010,17(5):056303.

[21] MCBRIDE R D,SLUTZ S A,JENNINGS C A,et al. Penetrating radiography of imploding and stagnating beryllium liners on the *Z* accelerator [J]. Physical Review Letters,2012,109(13):135004.

[22] LORENZ K T,EDWARDS M J,GLENDINNING S G,et al. Accessing ultrahigh-pressure,quasi-isentropic states of matter [J]. Physics Plasmas,2005,12(5):056309.

[23] REMINGTON B A,PARK H S,PRISBREY S T,et al. Progress towards materials science above 1000 GPa (10 Mbar) on the NIF laser:LLNL-CONF-411555 [R]. Livermore,CA:Lawrence Livermore National Laboratory,2009.

[24] BELOF J L,CAVALLO R M,OLSON R T,et al. Rayleigh-Taylor strength experiments of the pressure-induced phase transition in iron: LLNL-PROC-492911 [R]. Livermore, CA: Lawrence Livermore National Laboratory, 2011.

[25] PIRIZ A R, LÓPEZ CELA J J, TAHIR N A. Richtmyer-Meshkov instability as a tool for evaluating material strength under extreme conditions [J]. Nuclear Instruments and Methods in Physics Research Section A, 2009, 606(1/2):139-141.

[26] ATCHISON W L, ZOCHER M A, KAUL A M. Studies of material constitutive behavior using perturbation growth in explosive and magnetically driven liner systems [J]. Russian Journal of Physical Chemistry B, 2008, 2(3):387-401.

[27] PARK H S,BARTON N,BELOF J L,et al. Experimental results of tantalum material strength at high pressure and high strain rate [C]//AIP Conference Proceedings,2012,1426(1):1371-1374.

[28] BAI J S,WANG B,WANG T,et al. Numerical simulation of the Richtmyer-Meshkov instability in initially nonuniform flows and mixing with reshock [J]. Physical Review E,2012,86(6):066319.

[29] WANG T,TAO G,BAI J S,et al. Numerical comparative analysis of Richtmyer-Meshkov instability simulated by different SGS models [J]. Canadian Journal of Physics,2015,93(5):519-525.

[30] WANG T,LI P,BAI J S,et al. Large-eddy simulation of the Richtmyer-Meshkov instability [J]. Canadian Journal of Physics,2015,93(10):1124-1130.

爆轰驱动铝飞层扰动增长的数值模拟

王　涛[1,2],柏劲松[1],曹仁义[1],汪　兵[1],
钟　敏[1],李　平[1],陶　钢[2]

(1. 中国工程物理研究院流体物理研究所,四川 绵阳　621999;
2. 南京理工大学能源与动力工程学院,江苏 南京　210094)

摘要:建立了研究炸药爆轰驱动条件下金属材料 Rayleigh-Taylor 不稳定性问题的实验技术和数值模拟方法。利用该实验技术和数值模拟方法研究了炸药爆轰驱动条件下,铝飞层界面 Rayleigh-Taylor 不稳定性增长规律,数值模拟显示界面扰动振幅以指数规律增长。数值模拟结果和实验定性相符,但是定量相比有较大差别,原因是高压高应变率加载条件下铝的强度增强,而数值模拟时所采用的 SG 本构模型在这样的加载条件下低估了铝的强度而导致对扰动增长致稳作用不足。然后在数值模拟中,通过改变材料的初始剪切模量和初始屈服强度,发现在一定范围内,初始剪切模量对材料动态屈服强度没有影响,而初始屈服强度增大可以明显提高材料的动态屈服强度,达到抑制扰动增长的目的,表明材料屈服强度主导界面扰动增长。

关键词:爆轰驱动;Rayleigh-Taylor 不稳定性;扰动增长;材料强度;致稳

中图分类号:O33;O344.3　　**文献标志码**:A

doi:10.11858/gywlxb.20170624